

Published in final edited form as:

J Mol Biol. 2014 February 6; 426(3): 510–525. doi:10.1016/j.jmb.2013.09.043.

The oligomeric state of the active Vps4 AAA ATPase

Nicole Monroe¹, Han Han¹, Malgorzata D. Gonciarz^{1,2}, Debra M. Eckert¹, Mary Anne Karren¹, Frank G. Whitby¹, Wesley I. Sundquist^{1,*}, and Christopher P. Hill^{1,*}

¹Department of Biochemistry, University of Utah School of Medicine, 15 N Medical Drive East RM 4100, Salt Lake City, UT 84112-5650, USA

Abstract

The cellular ESCRT pathway drives membrane constriction toward the cytosol and effects membrane fission during cytokinesis, endosomal sorting, and the release of many enveloped viruses, including HIV. A component of this pathway, the AAA ATPase Vps4, provides energy for pathway progression. Although it is established that Vps4 functions as an oligomer, subunit stoichiometry and other fundamental features of the functional enzyme are unclear. Higher-order oligomers have thus far only been characterized for a Walker B mutant of Vps4 in the presence of ATP. Here, we report that although some mutant Vps4 proteins form dodecameric assemblies, active wild-type *S. cerevisiae* and *S. solfataricus* Vps4 enzymes can form hexamers in the presence of ATP and ADP, as assayed by size exclusion chromatography and equilibrium analytical ultracentrifugation. The Vta1p activator binds hexameric yeast Vps4p without changing the oligomeric state of Vps4p, implying that the active Vta1p:Vps4p complex also contains a single hexameric ring. Additionally, we report crystal structures of two different archaeal Vps4 homologs, whose structures and lattice interactions suggest a conserved mode of oligomerization. Disruption of the proposed hexamerization interface by mutagenesis abolished the ATPase activity of archaeal Vps4 proteins and blocked Vps4p function in *S. cerevisiae*. These data challenge the prevailing model that active Vps4 is a double ring dodecamer, and argue that, like other type I AAA ATPases, Vps4 functions as a single ring with six subunits.

Keywords

multivesicular body; HIV budding; ESCRT; AAA ATPase; protein oligomerization; X-ray crystallography

Introduction

The ESCRT (Endosomal Sorting Complexes Required for Transport) pathway mediates multiple cellular membrane remodeling and fission events including the abscission step of cytokinesis^{1; 2; 3}, formation of intraluminal vesicles that bud into the MVB (multivesicular

© 2013 Elsevier Ltd. All rights reserved.

*Corresponding authors: Name: Christopher P. Hill, chris@biochem.utah.edu, Phone: +1-801-585-5536, Fax: +1-801-581-7959. Name: Wesley I. Sundquist, wes@biochem.utah.edu, Phone: +1-801-585-5402, Fax: +1-801-581-7959.

²Present Address: Lilly Corporate Center, Indianapolis, IN 46285, USA

Accession numbers

Atomic coordinates and structure factors have been deposited in the Protein Data Bank with accession codes PDB ID: 4LGM for SsoVps4(E206Q, 85-372) and PDB ID: 4LCB for AhoVps4.

Publisher's Disclaimer: This is a PDF file of an unedited manuscript that has been accepted for publication. As a service to our customers we are providing this early version of the manuscript. The manuscript will undergo copyediting, typesetting, and review of the resulting proof before it is published in its final citable form. Please note that during the production process errors may be discovered which could affect the content, and all legal disclaimers that apply to the journal pertain.

body)^{4; 5; 6; 7; 8; 9}, and exosome and shedding microvesicle formation^{10; 11; 12}. This cellular pathway is exploited by retroviruses and many other enveloped viruses to facilitate budding and release from cells, a process that requires the same membrane topological changes as the endogenous cellular processes^{13; 14; 15; 16; 17; 18}. The ESCRT pathway has multiple components that act both early and late in vesiculation and membrane fission. The leading model is that ESCRT-III subunits drive the late stages by assembling into polymeric filaments that constrict the neck of the budding virus or vesicle^{19; 20; 21}. The only core enzyme in the pathway, Vps4 (vacuolar protein sorting 4), also performs an essential role by disassembling ESCRT-III filaments, a process that may be mechanistically coupled with membrane fission^{22; 23; 24; 25}. Although the ESCRT pathway has been primarily characterized in eukaryotic cells, homologs of Vps4 and its substrates have been identified in archaeal species belonging to the Sulfolobales or Desulfurococcales orders of the large crenarchaeal phylum^{26; 27}, where they mediate cleavage furrow ingression and cytokinesis^{28; 29}. Thaumarchaea and certain species of the euryarchaeal phylum also contain ESCRT-III and Vps4 homologs in addition to homologs of the bacterial cell division protein FtsZ²⁷. Similar to their eukaryotic counterparts, archaeal ESCRT proteins may also serve as host factors for the release of viruses that infect these organisms^{30; 31}.

Vps4 is a member of the meiotic clade of AAA ATPases^{32; 33; 34} (ATPases Associated with diverse cellular Activities). These enzymes typically comprise a variable N-terminal substrate-binding domain followed by either one or two ATPase cassettes (Type I and II AAA ATPases, respectively), each of which includes a large N-terminal domain and a smaller C-terminal domain. Vps4 is characterized by the presence of an N-terminal MIT (Microtubule Interacting and Trafficking) domain, a canonical ATPase cassette, and a C-terminal helix that packs against the large ATPase domain (Supplementary Figure 1). MIT domains are three-helix bundles that recognize different peptide motifs, termed MIM (MIT domain Interacting Motifs) located in the C-terminal tails of their ESCRT-III substrates^{35; 36; 37; 38}. Eukaryotic Vps4 proteins also contain a three-strand insertion (termed the β -domain) following the third helix of the small ATPase domain. This feature contributes to Vta1p/LIP5 binding^{39; 40; 41}, which stimulates Vps4 assembly and ATPase activity *in vitro*^{42; 43}, and promotes Vps4 activity *in vivo*^{26; 28; 29}. Although the Vta1p/LIP5 activator is important in eukaryotes, crenarchaeal Vps4 proteins lack a β -domain²⁶ and also lack recognizable Vta1/LIP5 proteins.

Eukaryotic Vps4 exhibits an inactive monomer-dimer equilibrium in the absence of nucleotides, and forms a functional higher-order oligomer upon binding ATP^{40; 44; 45; 46; 47; 48}. Obligate oligomerization is consistent with other AAA ATPases, which typically function as hexamers^{24; 25; 26}. Thus far, no crystal structures reported for Vps4 show closed rings, but in most cases show six-fold packing about a screw axis^{40; 45; 46; 48; 49}. Models for Vps4 assembly have therefore been guided by studies of its most closely related structural homologs, spastin⁵⁰ and p97^{51; 52; 53; 54}. We have previously proposed a model for a Vps4 hexamer⁴⁰ that was generated by superposition on the D1 ring of the type II AAA ATPase p97⁵² and supported by mutagenesis of proposed interface residues⁴⁵.

However, three independent electron microscopy studies have reported models for the assembled Vps4 protein that do not conform to a single ring hexamer. All three models feature a doubling structure with twelve^{47; 55} or fourteen⁴⁶ subunits, but otherwise differ considerably from each other in subunit organization. Owing to the stabilizing effects of nucleotide binding, these structural studies were all performed using either non-hydrolyzable ATP analogs⁴⁶ or the Vps4p(E233Q) mutant^{47; 55}. Equivalent E to Q variants are commonly used for studies of AAA ATPases because they bind but do not hydrolyze ATP

due to the requirement of the highly conserved glutamate to activate the water molecule that attacks the gamma phosphate^{56, 57}.

To clarify models of Vps4 assembly, we have determined the oligomeric state of the wild type protein in the presence of nucleotides. Surprisingly, although the *S. cerevisiae* Vps4p(E233Q) mutant enzyme can form a dodecamer, as reported previously^{40: 47}, we find that wild-type Vps4p assembles into a hexamer in the presence of nucleotides, and remains hexameric when associated with Vta1p. In contrast to an earlier report²⁶, we also find that the Vps4 enzyme from the crenarchaeon *Sulfolobus solfataricus* displays ATPase activity and can assemble into a hexamer, although dodecameric assemblies can also form under non-physiological conditions. To better understand crenarchaeal Vps4, we determined crystal structures of the ATPase domains of Vps4 proteins from *Sulfolobus solfataricus* and *Acidianus hospitalis*. These structures lack β -domains but otherwise closely resemble the eukaryotic proteins, validating their designation as Vps4 homologs. Although these Vps4 proteins did not crystallize as discrete hexamers, they did form lattices with six-fold screw axes that suggest models for the interfaces in the ring hexamer. Disruption of proposed interfaces prevents hexamerization in solution and abolishes ATPase activity, further supporting the p97-based homology model. Equivalent point mutations indicate that Vps4p hexamerization is required for MVB sorting in yeast, also supporting our model that Vps4 functions as a hexamer that resembles the D1 ring of p97.

Results

Wild-type *S. cerevisiae* Vps4p is a hexamer in the presence of nucleotides

Although wild-type Vps4p has not previously been reported to form stable assemblies, higher-order oligomerization is a prerequisite for Vps4p function⁴⁴. The enzyme is expected to achieve high local concentrations *in vivo* when its MIT domains bind the MIM motifs on the polymeric ESCRT-III filaments, and we therefore reasoned that wild-type Vps4p would oligomerize at high protein concentrations. Indeed, wild type Vps4p (100 μ M, 1 mM ATP) eluted from an analytical size exclusion column as a complex with an apparent molecular weight that approximated a hexamer (apparent MW = 245 kDa, calculated MW = 289 kDa, Figure 1A, panel 1, red curve). The peak was asymmetric, however, and tailed toward smaller species, indicating that multiple Vps4p complexes might be present in rapid exchange. Consistent with this possibility, the retention time of the Vps4p oligomer increased when the protein concentration was reduced (Figure 1B). Vps4p also formed hexamer-sized complexes in the presence of the non-hydrolyzable ATP analog ATP γ S (100 μ M Vps4p, 0.2 mM ATP γ S, Figure 1A, panel 2) and in the presence of ADP (100 μ M Vps4p, 1 mM ADP, Figure 1A, panel 3).

Consistent with previous reports that the hydrolysis-deficient Vps4p(E233Q) mutant dodecamerizes in the presence of ATP^{40: 47: 55}, we also found that ATP-bound Vps4p(E233Q) migrated more rapidly than the wild type protein (Figure 1A, panel 1, compare red and blue curves). In the presence of ADP, however, both the wild type and hydrolysis-deficient Vps4p proteins eluted as hexamer-sized complexes (Figure 1A, panel 3). These observations indicate: 1) Wild type yeast Vps4p oligomerizes reversibly into a higher-order complex that migrates primarily as an apparent hexamer on size exclusion chromatography; 2) Hexamerization is favored by high protein concentrations; 3) Unlike Vps4p(E233Q), wild type Vps4p does not form a stable dodecamer under our experimental conditions; 4) Vps4p and Vps4p(E233Q) can both form hexamer-sized complexes in the presence of ADP.

Equilibrium analytical ultracentrifugation (AUC) experiments were performed to obtain shape-independent estimates of the mass of the nucleotide-bound Vps4p complexes and to

determine their relative stabilities (Figure 1C). The non-hydrolyzable ATP analog, ATP γ S, was used in these experiments to avoid complications associated with ATP hydrolysis over the multiday centrifugation period. Importantly, ATP γ S-bound and ATP-bound Vps4p have indistinguishable size exclusion chromatography profiles (Figure 1A, compare panels 1 and 2). The AUC data could not be adequately fit using single-species models for Vps4p dimers, hexamers or dodecamers, but was adequately described by a dimer-hexamer equilibrium model with an equilibrium dissociation constant of 3.7 nM² when subunit concentrations up to 80 μ M were used. This dissociation constant implies that there will be equimolar concentrations of dimer and hexamer at a dimer concentration of 61 μ M, in reasonable agreement with the size exclusion chromatography data shown in Figure 1. At higher concentrations (100–120 μ M), the appearance of higher molecular weight species led to significant residual bias. Our attempts to globally fit all data using a dimer-dodecamer or a dimer-hexamer-dodecamer equilibrium did not produce satisfactory residuals, but the fits did indicate that the fraction of Vps4p forming higher molecular weight species was small under these conditions. Based on the 3.7 nM² K_D estimated from centrifugation, we conclude that the nucleotide-bound Vps4p size exclusion chromatography peaks represent rapidly equilibrating mixtures that initially consist of an approximately equimolar distribution of Vps4p subunits between hexamers and dimers in a ratio of 41:59 hexamer:dimer at the initial concentration of Figure 1A, panel 2, and that small amounts of larger species appear at higher concentrations.

We also used equilibrium AUC to analyze the oligomeric state of Vps4p in the presence of ADP to determine if there is a difference in the stability of the complex in the presence of different nucleotides (Figure 1D). Again, the radial distribution is best described by a dimer-hexamer equilibrium, this time with a much tighter dissociation constant of 0.04 nM². This result challenges the concept that Vps4p oligomers only form in the presence of ATP.

***S. cerevisiae* Vps4p remains hexameric upon binding of Vta1p**

Vta1p stimulates Vps4p ATPase activity *in vitro* at least in part by promoting Vps4p assembly³⁹. We therefore tested the effect of adding equimolar concentrations of Vta1p to Vps4p (100 μ M, 1 mM ATP). The Vps4p-Vta1p-ATP complex eluted as a single major peak (Figure 2A, red curve) that contained both proteins (Figure 2B) and had an apparent molecular weight of 520 kDa. We have previously shown that Vps4p(E233Q) and Vta1p form a stable 12:6 complex⁵⁵ (expected MW \approx 800 kDa). We verified this finding (Figure 2A, blue curve, apparent MW \approx 910 kDa), confirming that the ATP-bound complex of wild type Vps4p-Vta1p is substantially smaller than the ATP-bound complex of Vps4p(E233Q)-Vta1p. These observations indicate that wild type Vps4p remains hexameric when bound to Vta1p because the complex is significantly smaller than the Vps4p(E233Q)-Vta1p complex.

Our efforts to determine the stoichiometry of the Vps4p-Vta1p complex were complicated by the poor separation of complex and unbound protein. Moreover, the relatively weak affinity of Vta1p for its binding site on Vps4p (17 μ M⁴¹), combined with the Vps4p self-association, produced a complicated mixture of species during the size exclusion chromatography. Therefore, although both elution volume and band intensity suggest a 6:6 stoichiometry, we cannot rule out the possibility that the Vps4p hexamer can bind up to six Vta1p dimers, resulting in a 6:12 subunit stoichiometry⁴¹.

Oligomeric state of crenarchaeal Vps4 homologs

Owing to the complexity of *S. cerevisiae* Vps4p oligomerization, we also examined the oligomerization behavior of simpler Vps4 proteins from the hyperthermophilic crenarchaeal species, *Sulfolobus solfataricus* (SsoVps4; 36 % amino acid identity with human VPS4B, 35 % identity with *S. cerevisiae* Vps4p) and *Acidianus hospitalis* (AhosVps4; 36 % identity

with human VPS4B, 37 % identity with *S. cerevisiae* Vps4p). Primary sequences indicate that the crenarchaeal homologs lack a β -domain and do not associate with Vta1/LIP5 activators. Curiously, an earlier study concluded that recombinant SsoVps4 does not oligomerize²⁶. This prompted us to consider the possibility that these thermophilic proteins might need to be heated in order to oligomerize. We found that this is indeed the case, and therefore incubated the Sso and AhoS proteins for 15 minutes at 75 °C during the purification procedure (see materials and methods).

In the absence of nucleotide, both wild-type SsoVps4 and the hydrolysis mutant SsoVps4(E206Q) appeared to be dodecameric as analyzed by size exclusion chromatography (Figure 3 A, panel 1, compare red and blue traces). This is similar to a report of the Vps4 homolog CdvC from *Metallosphaera sedula*, which forms dodecamer-sized oligomers in the absence of nucleotides⁵⁸. In the presence of ATP or ADP, however, both wild type and E206Q SsoVps4 eluted as lower molecular weight complexes, whose retention times were close to those expected for hexamers (Figure 3A, panels 2 and 3). SsoVps4(E206Q) eluted slightly earlier than the wild-type protein, and both proteins migrated slightly more rapidly when bound to ADP than ATP. AhoSVps4 behaved similarly to SsoVps4, both in the absence and presence of nucleotide (Supplementary Figure 2 and data not shown).

Like *S. cerevisiae* Vps4p, the archaeal proteins eluted in asymmetric peaks, suggesting that the protein is rapidly interconverting between multiple oligomeric states. Consistent with this hypothesis, the retention volume of ATP-bound SsoVps4 decreased as the concentration increased (Figure 3B, panel 1). Note that the peak maximum shifted to retention volumes of larger apparent molecular weight than a hexamer when concentrations higher than 100 μ M were used. Because SsoVps4 will only oligomerize if the protein is exposed to elevated temperatures at least once during the purification procedure, we tested the effect of temperature on the migration behavior of SsoVps4 by performing similar size exclusion chromatography experiments at room temperature (Figure 3C, panels 2 and 3). For each concentration analyzed, the protein migrated more rapidly at room temperature than at 4 °C, indicating that oligomerization is entropically driven.

Analytical ultracentrifugation analyses of SsoVps4

AUC was used to obtain shape-independent measures of the sizes and equilibria of SsoVps4. In the absence of nucleotide, the radial distribution fit a single species dodecamer model (Figure 4A) for the E206Q mutant. This analysis was also performed in the presence of 1 mM ATP, which was possible because ATPase activity was negligible at 4 °C. The equilibrium distribution of SsoVps4 in the presence of ATP could not be adequately fit by a single species model, and the best fit was obtained using a dimer-hexamer model with a K_D of 0.01 nM² (Figure 4B). We therefore conclude that the nucleotide-bound SsoVps4 size exclusion chromatography peaks represent rapidly interconverting mixtures of hexamers and dimers, although in this case the hexamer predominates because the estimated K_D implies that SsoVps4 subunits initially partition into a ratio of 89:11 hexamer:dimer during size exclusion chromatography (Figure 3A, panel 2). Thus, despite their evolutionary divergence, Vps4 proteins from both yeast and crenarchaea can form stable dodecamers under some conditions, but in both cases the wild type Vps4 enzymes interconvert between dimers and hexamers in the presence of adenosine nucleotides.

We performed similar sedimentation equilibrium experiments on AhoSVps4. However, this protein was more polydisperse and tended to form higher-order aggregates, and we were therefore not able to fit to random residuals.

ATPase activity of archaeal Vps4 proteins

Although sequence alignments show the presence of Walker A, Walker B and sensor 1 motifs that are typical of authentic AAA ATPases (Supplementary Figure 1), there is a report that SsoVps4 lacks ATPase activity²⁶. The results of an ATPase activity assay have not been reported for AhosVps4. Our observation that the recombinant Vps4 homologs of *S. solfataricus* and *A. hospitalis* form higher-order oligomers upon heat treatment prompted us to test whether these proteins are functional ATPases at different temperatures. As shown in Figure 5, ATP hydrolysis was not detected at 4 °C or 37 °C, but both SsoVps4 and AhosVps4 displayed strong ATPase activity at 60 °C. The rate of ATP hydrolysis was 16.8 ATP/min/subunit for SsoVps4 at an enzyme concentration of 0.5 μM, and 67 ATP/min/subunit for AhosVps4 at 0.2 μM. As expected, mutation of the Walker B glutamate abolished enzymatic activity in the point mutants SsoVps4(E206Q) and AhosVps4(E200Q) (Figure 5). Consistent with our results, a previous study found a maximal ATP hydrolysis rate of 210 ATP/min/subunit (reported as 0.5 μmol ATP/min per mg) for the Vps4 homolog from the hyperthermophilic archaeon *Metallosphaera sedula*⁵⁸ at the same temperature. The requirement for high temperature is consistent with the observation that increasing temperature drives oligomerization (above) and because these proteins have been evolutionarily optimized to function at elevated temperature⁵⁹.

Crystal structures of Vps4 proteins from *S. solfataricus* and *A. hospitalis*

Motivated by the observation that crenarchaeal Vps4 proteins oligomerize more tightly without the requirement for an activator protein, we determined crystal structures of SsoVps4 and AhosVps4 in the absence of nucleotide. Unfortunately, neither structure appears to capture an active arrangement. Data collection and refinement statistics are listed in Table 1. SsoVps4 crystals were grown from a construct spanning the ATPase domain (residues 85-372) containing the E206Q mutation. Diffraction data were collected to a resolution of 2.8 Å, the structure was determined by the SAD method, and the model was refined to an R_{free} value of 27 %. Most of the sequence for residues 99–369 is ordered and reveals an AAA ATPase cassette that closely resembles previously reported structures of eukaryotic Vps4 proteins (Figure 6A). Superposition of the SsoVps4(E206Q) ATPase domain (green) with yeast Vps4p (PDB ID: 3EIE⁴⁵, blue) yields a root-mean-square deviation of 1.622 Å on 237 pairs of C α atoms. We also crystallized wild-type, full-length AhosVps4, determined the structure by molecular replacement using our refined SsoVps4 structure as a search model, and refined the model to an R_{free} value of 26 % against data to a resolution of 2.1 Å. Although SDS-PAGE analysis of washed crystals confirmed that the crystals contained the intact protein (Supplementary Figure 3), the MIT domain and linker are not visible in electron density maps, presumably due to disorder. Most of the sequence corresponding to residues 93–362, which covers the ATPase cassette of AhosVps4, is well ordered. Consistent with their 75 % amino acid sequence identity, the AhosVps4 and SsoVps4 ATPase cassette structures superimpose closely, with a root-mean-square deviation of 0.492 Å on 206 pairs of C α atoms (Figure 6B).

All five helices of the eukaryotic large AAA ATPase domain and four helices of the small AAA ATPase domain have counterparts in the crenarchaeal proteins. We found a minor difference, in that the human, mouse and yeast Vps4 ATPase cassette structures each contain six β -strands in the large AAA ATPase domain, whereas both of our archaeal Vps4 structures display only five β -strands, and the residues that correspond to the eukaryotic β' strand are disordered in archaea. Also, as anticipated from sequence alignments (Supplementary Figure 1), the ~45 residue β -domain that is inserted between helix 8 and 9 in eukaryotic Vps4 proteins is missing from the SsoVps4 and AhosVps4 AAA ATPase cassettes. Instead, the two helices are connected by a well-ordered loop.

Analysis of the crystallographic interface

None of the crystal structures reported to date directly reveals how the active Vps4 oligomer is assembled. We have previously presented mutagenesis data that implicate an interface seen in crystal forms of yeast Vps4p as being important for assembly⁴⁵. Remarkably, this interface, which propagates the crystallographic or non-crystallographic 6₅ screw axis seen in all published yeast Vps4p crystal structures^{43; 45; 46} and all reported structures of human and murine VPS4B^{40; 49}, is also found in SsoVps4 and AhoVps4 crystals, where it propagates 6₄ and 6₅ screw axes, respectively. Despite the difference in helical pitch, the ~600 Å² interfaces are highly similar in SsoVps4 and AhoVps4 crystals. The majority of the interface is formed by residues in helix 1 of the large AAA ATPase domain packing against helix 8 of the small AAA ATPase domain, and superposition of 13 pairs of Ca atoms from helices 1 and 8 across the SsoVps4 and AhoVps4 interfaces yields an RMSD of 1.2 Å. The interface residues are highly conserved throughout crenarchaea and, as seen in many functional interfaces⁶⁰, central hydrophobic residues are flanked by polar interactions.

Guided by our earlier analysis of yeast Vps4p interfaces and the observation that packing of SsoVps4 and AhoVps4 resembles packing of the closed hexameric ring of p97 D1 when viewed along the screw axis (Figure 7A), we propose a Vps4 hexamer model that resembles p97 D1. The conserved subunit interfaces are very similar to those seen in the crystal, differing only in a combination of subunit rotation (~15–20°) and slight adjustment of interdomain angles (~6°). This model is very similar to the model we proposed earlier for yeast and human Vps4^{40; 45}. To test the proposal that the crystallographic interface resembles the hexamer interface of crenarchaeal Vps4 proteins, we mutated SsoVps4 residues Tyr121 and Phe328, which form a π -stacking interaction at the core of the interface, to Asp and Ala, respectively. Size exclusion chromatography revealed that both of these variant proteins migrated more slowly than wild-type Vps4p in the presence of ATP (Figure 7C). SsoVps4(F328A) eluted as a dimer, whereas SsoVps4(Y121D) eluted in a broad peak with a maximum between the expected retention volumes of a dimer and a hexamer. Consistent with its diminished self-association, SsoVps4(F328A) retains only 20 % of wild type ATPase activity, whereas SsoVps4(Y121D) has negligible ATPase activity, which suggests that the residual assembly may be non-native (Figure 7D). As shown in Figure 8A, the packing generates a complete AAA ATPase active site geometry, including SsoVps4 Arg262, which is structurally equivalent to the arginine finger residue of many AAA ATPases⁵⁷. Consistent with this model, the mutant SsoVps4(R262A) protein displays diminished hexamerization and fails to hydrolyze ATP (Figures 8B and 8C). The adjacent residue, Arg263, is also a candidate for the arginine finger, and its mutation to alanine similarly diminishes assembly and activity. This reflects a similar situation to p97, where both AAA ATPase cassettes contain two arginine residues in close proximity to the active site^{51; 61}.

Functional relevance of the p97-like hexamer in *S. cerevisiae*

We have previously described mutations that disrupt higher-order assembly of *S. cerevisiae* Vps4p(E233Q). Specifically, each of the Vps4p(E233Q) L151D, I351A and I354D point mutant proteins are monomeric⁴⁵, and the Vps4p(E233Q, R352A) mutant is dimeric in solution⁴⁰. All of these mutations map to the interface between neighboring subunits in our p97-based model of the assembled Vps4p hexamer⁴⁰ (Figure 9A). As shown in Figure 9B, we found that the L151D and R352A mutations also disrupted higher-order oligomerization of wild type Vps4p.

We tested these two hexamerization mutants for the ability to support the ESCRT-dependent sorting of a model GFP-CPS cargo into yeast multivesicular bodies (MVBs)³⁶ (Figure 9C).

When the ESCRT pathway is functional, GFP-CPS is sorted into MVB vesicles and concentrates within the vacuole, and the lumen fluoresces green (Figure 9C, inset, upper panel). In the absence of ESCRT pathway activity, the GFP-CPS cargo is not sorted into MVB vesicles, resulting in green fluorescent labeling of the limiting vacuolar membrane (Figure 9C, inset, lower panel). The ESCRT pathway requires Vps4p activity, and these two different phenotypes are therefore observed in yeast cells that either express or lack wild type Vps4p. Each of the phenotypes was highly penetrant, as reflected in the scoring of 3× 100 cells that either expressed wild type Vps4p (95.1 ± 2.4 % of cells exhibited luminal GFP staining) or lacked Vps4p (1.1 ± 1.9 % of cells exhibited luminal staining). To determine the importance of hexamerization, GFP-CPS sorting was scored in cells that expressed either monomeric Vps4p(L151D) (2.0 ± 1.0 % of cells exhibiting vacuolar membrane staining) or dimeric Vps4p(R352A) (2.5 ± 2.1 % of cells exhibiting vacuolar membrane staining). The expression level of Vps4p was not significantly affected by the point mutations, and was similar to the level of endogenous Vps4p (data not shown). Thus, two different point mutations that disrupt the formation of the p97-like Vps4p hexamer *in vitro* also inhibit Vps4p function in MVB protein sorting in yeast.

Discussion

Vps4 is a key component of the cellular ESCRT pathway. To understand how conformational changes during the ATP hydrolysis cycle translate into remodeling of the ESCRT-III polymer, it is critical to define the quaternary structure of the active Vps4 enzyme. Previous reports have described Vps4p as a double ring structure because biophysical characterization of the *S. cerevisiae* Vps4p(E233Q) mutant suggested that the assembled enzyme contained 10–14 subunits. This hypothesis was supported by three independent EM reconstructions that all contained two stacked rings with six-fold^{47; 55} or seven-fold⁴⁶ symmetry, although in other regards the EM reconstructions were dramatically different from one another. The suggested double ring structure also differed from other type I AAA ATPases like spastin, which form a single hexameric ring⁵⁰. Type II AAA ATPases such as p97 do have two stacked rings, but the double-ring architecture results from a hexameric subunit arrangement with each subunit contributing two AAA ATPase domains⁵⁴.

The data presented here show that wild-type yeast and archaeal Vps4 proteins exist in equilibrium between oligomeric states, and at sufficiently high concentration in the presence of nucleotide assemble into hexamers and other higher-order oligomers. These findings are consistent with the concentration-dependence of ATP hydrolysis rates that we and others^{39; 44; 62} have observed *in vitro*, and support a model for Vps4 activation in which the high local concentration that results from recruitment to ESCRT-III polymers, together with activation by LIP5/Vta1, drives assembly into an active complex^{63; 64}. The distribution of oligomeric states that we observe for wild-type Vps4 *in vitro* raises the question: Which one represents the biologically active species? AAA ATPases most commonly function as hexameric assemblies^{65; 66; 67}, but can sometimes also exist in oligomeric states other than that of their functional unit. For example: 1) The ClpB AAA ATPase switches from a predominantly heptameric assembly to a hexamer upon nucleotide binding⁶⁸; 2) The archaeal proteasome activating nucleosidase PAN exists as a dodecamer when overexpressed in bacteria⁶⁹, but functions as a hexamer⁷⁰; 3) RuBisCO activase exists in a concentration-dependent distribution of oligomeric states⁷¹, but a point mutation can convert the enzyme into functional hexamers⁷².

In the case of yeast Vps4p, the hydrolysis-deficient protein, Vps4p(E233Q), is dodecameric in the presence of ATP. We suggest that this assembly may be artifactual, however, because the oligomerization behavior of Vps4p(E233Q) in the presence of ATP differs from that of

the wild-type protein. Replacing the conserved Walker B glutamate by a glutamine is common in studies of ATPases because it allows ATP binding and assembly, while preventing hydrolysis⁵⁷. Indeed, there are no significant differences between the crystal structures of unassembled wild-type and hydrolysis-deficient Vps4p enzymes, nor do these proteins differ in dimerization behavior⁴⁵. Moreover, mixed complexes of wild-type Vps4p and Vps4p(E233Q) retain ATPase activity^{44; 62}. Nevertheless, our data indicate that ATP stabilizes Vps4p(E233Q) in a dodecameric assembly under conditions where the wild-type protein is predominantly hexameric.

Crystal structures of RecA-like and AAA+ hexameric helicases in complex with substrates indicate that ring asymmetry is fundamental to mechanism^{73; 74}. Similarly, we propose that wild-type Vps4 forms a closed hexameric ring, with ring closure accommodated by different conformations within the subunits around the ring. In this model, the conformational variability results from alternative flexing between large and small ATPase domains that is induced by different ATP/ADP nucleotide binding states and therefore varies throughout the reaction cycle. This hypothesis is supported by crystal structures of Vps4p that suggest a nucleotide-dependent change in the angle between the large and small AAA ATPase domains^{45; 48}. When ATP is bound to hydrolysis-deficient Vps4p(E233Q), subunits may be forced into the same nucleotide state, thereby artificially restricting its ability to assume the active asymmetric assembly. The resulting aberrant hexamer may present surfaces that stabilize non-native ring stacking. The second acidic residue in the Walker B motif, which corresponds to Glu233 in Vps4p, forms an inter-subunit salt bridge in p97 and NSF⁷⁵ except when this interaction is displaced by the γ -phosphate of bound ATP. Given the assumption that native assembly requires different nucleotide states, Vps4p(E233Q) may form aberrant assemblies because subunits that are not bound to ATP cannot adopt a native non-ATP state. A requirement for different nucleotide states could also explain why we have not observed dodecamer formation upon binding of non-hydrolyzable ATP γ S to the wild-type enzyme. Interestingly, the equivalent mutation does not seem to significantly affect oligomerization in archaeal proteins. In short, while we cannot fully explain the assembly of Vps4p(E233Q), we have focused our studies on the more relevant wild-type protein.

Our data support the model that the hexamer is the smallest functional unit of the Vps4 enzyme. The following observations support the relevance of a p97-like hexameric ring structure: (1) Wild-type Vps4 proteins from *S. cerevisiae*, *S. solfataricus* and *A. hospitalis* assemble into hexamers in the presence of nucleotide; (2) Wild-type Vps4p remains hexameric in complex with Vta1p activators; and (3) Conservation of the hexamer interface is suggested by crystal structures and by analyses of Vps4 point mutations that disrupt assembly *in vitro* and block ESCRT pathway function in yeast cells. Although we have not definitively determined a stoichiometry for the Vps4-Vta1 complex, structural studies indicate that each β -domain associates with a Vta1 dimer⁴¹. Our data do not indicate that binding of the Vta1 dimer to the β -domains at the periphery of Vps4 rings stabilizes interactions between hexamers as suggested by previous studies^{41; 43} insofar as we do not observe such assemblies in our size exclusion chromatography experiments (Figure 2A). Nevertheless, we cannot exclude the possibility that such clustering of hexamers may occur at the high local concentrations expected at the ESCRT-III lattice.

In addition to hexamers, we also observed a small fraction of larger complexes of *S. cerevisiae* and crenarchaeal wild-type Vps4. We do not know how the hexamers assemble further, or whether these structures are biologically relevant. The size of higher-order assemblies continues to increase with increasing protein concentration. One possible explanation for this observation is that non-native ring structures that form in the presence of a single type of nucleotide are prone to stacking interactions and give rise to double ring structures as described for Vps4p(E233Q). Alternatively, if ring closure cannot be

accomplished, subunits may be added to the ends of a spiral that may resemble the helical packing in the crystal lattice. A limitation of our *in vitro* studies is that they were performed in the absence of the ESCRT-III substrate, and further studies are needed to understand the effects of cofactor and substrate binding on the oligomerization state. The leading model is that substrates bind to the pore loops at the center of the Vps4 hexamer, and in doing so impart asymmetry upon the hexamer. Visualizing the Vps4 structure that binds substrate and learning how its asymmetry is coupled to progression of ATP binding and hydrolysis in the different subunits will be fundamental to understanding Vps4 mechanism. Nevertheless, our finding that the yeast and archaeal Vps4 proteins oligomerize in a concentration-dependent manner using a conserved hexamerization interface and that the wild type proteins form hexamers in the presence of ATP supports the model that Vps4 functions as a spastin-like⁵⁰ six-membered ring.

Materials and Methods

Protein expression and purification

S. cerevisiae Vps4p and Vta1p were expressed and purified as described^{40; 45}. The Vps4 gene (SSO0909) from *S. solfataricus* was amplified from genomic DNA (ATCC 35092D-5) and cloned into a pET151 vector (Invitrogen) encoding an N-terminal 6xHis-tag followed by a PreScission protease (GE Healthcare) cleavage site. The Vps4 gene from *A. hospitalis* was synthesized by DNA2.0 (Menlo Park, CA, USA) with the same cleavable N-terminal 6xHis-tag, and cloned into pJexpress414 (DNA2.0). Mutations were introduced by Quikchange mutagenesis (Stratagene). Plasmids for protein expression were deposited at the DNASU Plasmid Repository⁷⁶ (<http://dnasu.org/DNASU/>) (Supplementary Table 1).

SsoVps4 and AhoVps4 were expressed in *E. coli* BL21(DE3) RIL cells (Stratagene) grown in ZY autoinduction media at 37 °C for 6 hours and then at 19 °C overnight. Cells were pelleted by centrifugation, resuspended in lysis buffer (25 mM Tris/HCl pH 7.4, 450 mM NaCl, 20 mM imidazole, 1 mg/ml lysozyme, protease inhibitors) and incubated for 45 min on ice followed by sonication and clarification by centrifugation (15000 rpm, 45 min, 4 °C). The supernatant was incubated at 75 °C for 15 min, precipitated protein removed by centrifugation, and the soluble fraction bound to Ni-NTA agarose equilibrated with 25 mM Tris/HCl pH 7.4, 450 mM NaCl, and 20 mM imidazole. Following a wash with the same buffer, protein was eluted with 200 mM imidazole, dialyzed into 25 mM Tris/HCl pH 7.4, 150 mM NaCl, 1 mM EDTA and 1 mM DTT, and incubated with 1 mg His-tagged PreScission protease per 100 mg of protein overnight at 4°C to remove the N-terminal His-tag. Uncleaved protein and the protease were removed by batch-binding to Ni-NTA agarose. Cleaved Vps4 was further purified by size exclusion chromatography in 25 mM Tris/HCl pH 7.4, 100 mM NaCl using a Superdex S200 column.

Structure determination

Crystals were grown in the absence of nucleotide by sitting drop vapor diffusion at 20°C using protein in the size exclusion chromatography buffer. Selenomethionine-substituted SsoVps4(85-372, E206Q) crystals grew in drops composed of 1 µl of a 7 mg/ml protein stock solution and 2 µl of reservoir solution (70 % (v/v) MPD, 100 mM HEPES pH 7.5). AhoVps4 crystals grew in drops composed of 1.5 µl of 10 mg/ml protein mixed with 1.5 µl of reservoir solution (0.2 M MgCl₂, 0.1 M HEPES pH 7.5, 30 % (v/v) PEG400). In both cases, crystals were cryo-cooled for data collection by plunging into liquid nitrogen directly from the mother liquor.

Diffraction data were collected at beam lines 11-1 (AhoVps4) and 7-1 (SsoVps4(85-372, E206Q)) of the Stanford Synchrotron Radiation Lightsource and processed using the

HKL2000 suite⁷⁷. Phases for SsoVps4(85-372, E206Q) were determined by the SAD method using SOLVE⁷⁸. The AhoVps4 structure was determined by molecular replacement using PHASER⁷⁹ and the refined structure of SsoVps4(85-372, E206Q) as a search model. Both models were refined using Refmac⁸⁰ and Phenix with rounds of rebuilding in COOT⁸¹.

Interfaces were analyzed using PISA⁸² and structures superimposed using secondary structure matching (SSM)⁸³ as implemented in the CCP4 package⁸⁴. Figures of molecular structures were prepared in Pymol⁸⁵.

Analytical size exclusion chromatography

Size exclusion chromatography was performed at 4 °C unless otherwise stated. A Superdex 200 size exclusion column (GE Healthcare) was calibrated with molecular weight standards (Biorad). Protein samples at a concentration of 100 μM (unless indicated otherwise) were used for size exclusion chromatography in 25 mM Tris/HCl pH 7.4, 100 mM NaCl or in the same buffer supplemented with 2 mM magnesium chloride and 1 mM ATP, 1 mM ADP or 0.2 mM ATP γ S. For yeast proteins, the buffer was supplemented with 1 mM DTT. Archaeal proteins were analyzed in the absence of reductant because they contain only a single cysteine that is not exposed on the surface. Vps4 proteins were preincubated with the respective nucleotide at the concentration used in the size exclusion chromatography buffer for 5 min on ice prior to analysis.

Analytical Ultracentrifugation

Analytical ultracentrifugation experiments were performed using absorbance optics for nucleotide free experiments and Rayleigh interference optics in the presence of nucleotides to avoid complications from nucleotide absorbance. Equilibrium sedimentation experiments on SsoVps4(E206Q) in the absence of nucleotide were performed at 4 °C using an XL-A analytical ultracentrifuge (Beckman Coulter). Sample cells with a six-channel centerpiece were filled with 120 μl of the protein sample at concentrations ranging from 2.5 μM to 10 μM, and 125 μl of size exclusion chromatography buffer was loaded into the reference sectors. Absorbance scans at 280 nm were taken at equilibrium after centrifugation at 3500 rpm and 5000 rpm.

Sedimentation equilibrium experiments in the presence of nucleotides were performed using an XL-I analytical ultracentrifuge (Beckman Coulter). External loading cells with a 2-channel centerpiece were loaded with 140 μl of water and aged by alternate cycles of centrifugation at 8000 rpm and re-torquing until the cells were mechanically stable, after which blank scans were then taken at all speeds used for the experiment following a procedure described by Cole and colleagues⁸⁶. The water was then exchanged for 120 μl of protein samples at concentrations ranging from 10 to 50 μM in 25 mM Tris/HCl pH 7.4, 100 mM NaCl, 2 mM magnesium chloride supplemented with 1 mM ATP, ATP γ S or ADP with the corresponding buffer in the reference cell. Interference data were collected at 4 °C and rotor speeds of 3000 and 5000 rpm, and analyzed using the Heteroanalysis software (version 1.1.56)⁸⁷. Theoretical molecular weights and partial specific volumes were calculated in SEDNTERP (Version 1.09)⁸⁸ based on the amino acid sequence. To fit interference data, the extinction coefficient at 280 nm was converted to a refractive index increment using a factor of 2.75.

ATPase activity

ATPase activity of Vps4 proteins was measured as described for human VPS4A⁶⁴. Reactions containing 0.1–0.5 μM Vps4 in 25 mM Tris/HCl pH 7.4, 100 mM NaCl, 5 mM MgCl₂, and 1 mM ATP in a total volume of 50 μl proceeded for at least 5 min at the

temperature indicated (4, 37 or 60°C). The reaction was then placed on ice and quenched with 100 μ l of malachite green color reagent (14 mM ammonium molybdate, 1.3 M HCl, 0.1 % (v/v) Triton X-100, 1.5 mM malachite green) and 50 μ l of 21 % (w/v) citric acid. The green complex formed by malachite green, molybdate and free phosphate was detected by absorbance at 650 nm using a plate reader. A sodium phosphate standard curve was used to estimate the amount of phosphate released during ATP hydrolysis.

GFP-CPS sorting in yeast cells

Vacuolar cargo sorting assays were performed as described³⁶. Confocal microscopy was used to image *vps4p* Δ yeast cells in a SEY6210 genetic background harboring pRS415MET +GFP-CPS and either pRS416+Vps4p (WT or mutant) or an empty control plasmid. For each data set, 100 cells were scored for GFP fluorescence in the vacuolar lumen in three independent experiments. Limiting vacuolar membranes were stained with FM4-64.

Supplementary Material

Refer to Web version on PubMed Central for supplementary material.

Acknowledgments

We thank Markus Babst (University of Utah) and Janet Shaw (University of Utah) for antibody reagents. Portions of this work were performed in Core Facilities at the University of Utah, which were supported by P30CA042014 from the National Cancer Institute. Portions of this research were performed at the Stanford Synchrotron Radiation Lightsource (SSRL), a national user facility operated by Stanford University on behalf of the U.S. Department of Energy, Office of Basic Energy Sciences. The SSRL Structural Molecular Biology Program is supported by the Department of Energy, Office of Biological and Environmental Research, and the NIH, National Center for Research Resources, Biomedical Technology Program, and the National Institute of General Medical Sciences. N.M. was supported by grants PBZHP3-135952 and PBZHP3-141465 from the Swiss National Science Foundation. This work was supported by NIH grant P50 GM082545 to C.P.H. and W.I.S.

Abbreviations

AAA ATPase	ATPase associated with diverse cellular activities
ESCRT	endosomal sorting complexes required for transport
EM	electron microscopy
AUC	analytical ultracentrifugation
GFP	green fluorescent protein
CPS	carboxypeptidase S

References

1. Carlton JG, Martin-Serrano J. Parallels between cytokinesis and retroviral budding: a role for the ESCRT machinery. *Science*. 2007; 316:1908–12. [PubMed: 17556548]
2. Morita E, Sandrin V, Chung HY, Morham SG, Gygi SP, Rodesch CK, Sundquist WI. Human ESCRT and ALIX proteins interact with proteins of the midbody and function in cytokinesis. *EMBO J*. 2007; 26:4215–27. [PubMed: 17853893]
3. Caballe A, Martin-Serrano J. ESCRT machinery and cytokinesis: the road to daughter cell separation. *Traffic*. 2011; 12:1318–26. [PubMed: 21722282]
4. Babst M, Sato TK, Banta LM, Emr SD. Endosomal transport function in yeast requires a novel AAA-type ATPase, Vps4p. *EMBO J*. 1997; 16:1820–31. [PubMed: 9155008]
5. Bishop N, Woodman P. ATPase-defective mammalian VPS4 localizes to aberrant endosomes and impairs cholesterol trafficking. *Mol Biol Cell*. 2000; 11:227–39. [PubMed: 10637304]

6. Finken-Eigen M, Rohricht RA, Kohrer K. The VPS4 gene is involved in protein transport out of a yeast pre-vacuolar endosome-like compartment. *Curr Genet.* 1997; 31:469–80. [PubMed: 9211789]
7. Fujita H, Yamanaka M, Imamura K, Tanaka Y, Nara A, Yoshimori T, Yokota S, Himeno M. A dominant negative form of the AAA ATPase SKD1/VPS4 impairs membrane trafficking out of endosomal/lysosomal compartments: class E vps phenotype in mammalian cells. *J Cell Sci.* 2003; 116:401–14. [PubMed: 12482925]
8. Yoshimori T, Yamagata F, Yamamoto A, Mizushima N, Kabeya Y, Nara A, Miwako I, Ohashi M, Ohsumi M, Ohsumi Y. The mouse SKD1, a homologue of yeast Vps4p, is required for normal endosomal trafficking and morphology in mammalian cells. *Mol Biol Cell.* 2000; 11:747–63. [PubMed: 10679028]
9. Hanson PI, Cashikar A. Multivesicular body morphogenesis. *Annu Rev Cell Dev Biol.* 2012; 28:337–62. [PubMed: 22831642]
10. Deatherage BL, Cookson BT. Membrane vesicle release in bacteria, eukaryotes, and archaea: a conserved yet underappreciated aspect of microbial life. *Infection and immunity.* 2012; 80:1948–57. [PubMed: 22409932]
11. Nabhan JF, Hu R, Oh RS, Cohen SN, Lu Q. Formation and release of arrestin domain-containing protein 1-mediated microvesicles (ARMMs) at plasma membrane by recruitment of TSG101 protein. *Proc Natl Acad Sci U S A.* 2012; 109:4146–51. [PubMed: 22315426]
12. Wehman AM, Poggioli C, Schweinsberg P, Grant BD, Nance J. The P4-ATPase TAT-5 inhibits the budding of extracellular vesicles in *C. elegans* embryos. *Current biology : CB.* 2011; 21:1951–9. [PubMed: 22100064]
13. Bieniasz PD. Late budding domains and host proteins in enveloped virus release. *Virology.* 2006; 344:55–63. [PubMed: 16364736]
14. Fujii K, Hurley JH, Freed EO. Beyond Tsg101: the role of Alix in ‘ESCRTing’ HIV-1. *Nat Rev Microbiol.* 2007; 5:912–6. [PubMed: 17982468]
15. Morita E, Sundquist WI. Retrovirus budding. *Annu Rev Cell Dev Biol.* 2004; 20:395–425. [PubMed: 15473846]
16. Welsch S, Muller B, Krausslich HG. More than one door - Budding of enveloped viruses through cellular membranes. *FEBS Lett.* 2007; 581:2089–97. [PubMed: 17434167]
17. Weiss ER, Gottlinger H. The role of cellular factors in promoting HIV budding. *J Mol Biol.* 2011; 410:525–33. [PubMed: 21762798]
18. Martin-Serrano J, Neil SJ. Host factors involved in retroviral budding and release. *Nat Rev Microbiol.* 2011; 9:519–31. [PubMed: 21677686]
19. Bodon G, Chassefeyre R, Pernet-Gallay K, Martinelli N, Effantin G, Hulsik DL, Belly A, Goldberg Y, Chatellard-Causse C, Blot B, Schoehn G, Weissenhorn W, Sadoul R. Charged multivesicular body protein 2B (CHMP2B) of the endosomal sorting complex required for transport-III (ESCRT-III) polymerizes into helical structures deforming the plasma membrane. *The Journal of biological chemistry.* 2011; 286:40276–86. [PubMed: 21926173]
20. Effantin G, Dordor A, Sandrin V, Martinelli N, Sundquist WI, Schoehn G, Weissenhorn W. ESCRT-III CHMP2A and CHMP3 form variable helical polymers in vitro and act synergistically during HIV-1 budding. *Cellular microbiology.* 2013; 15:213–26. [PubMed: 23051622]
21. Hanson PI, Roth R, Lin Y, Heuser JE. Plasma membrane deformation by circular arrays of ESCRT-III protein filaments. *J Cell Biol.* 2008; 180:389–402. [PubMed: 18209100]
22. Henne WM, Buchkovich NJ, Emr SD. The ESCRT pathway. *Dev Cell.* 2011; 21:77–91. [PubMed: 21763610]
23. Hurley JH. The ESCRT complexes. *Critical Reviews in Biochemistry and Molecular Biology.* 2010; 45:463–87. [PubMed: 20653365]
24. Hill CP, Babst M. Structure and function of the membrane deformation AAA ATPase Vps4. *Biochim Biophys Acta.* 2012; 1823:172–81. [PubMed: 21925211]
25. McCullough J, Colf LA, Sundquist WI. Membrane Fission Reactions of the Mammalian ESCRT Pathway. *Annual review of biochemistry.* 2013; 82:663–92.
26. Hobel CF, Albers SV, Driessen AJ, Lupas AN. The *Sulfolobus solfataricus* AAA protein Sso0909, a homologue of the eukaryotic ESCRT Vps4 ATPase. *Biochem Soc Trans.* 2008; 36:94–8. [PubMed: 18208393]

27. Makarova KS, Yutin N, Bell SD, Koonin EV. Evolution of diverse cell division and vesicle formation systems in Archaea. *Nat Rev Microbiol.* 2010; 8:731–41. [PubMed: 20818414]
28. Lindas AC, Karlsson EA, Lindgren MT, Ettema TJ, Bernander R. A unique cell division machinery in the Archaea. *Proc Natl Acad Sci U S A.* 2008; 105:18942–6. [PubMed: 18987308]
29. Samson RY, Obita T, Freund SM, Williams RL, Bell SD. A role for the ESCRT system in cell division in archaea. *Science.* 2008; 322:1710–3. [PubMed: 19008417]
30. Snyder JC, Young MJ. Potential role of cellular ESCRT proteins in the STIV life cycle. *Biochem Soc Trans.* 2011; 39:107–10. [PubMed: 21265756]
31. Snyder JC, Samson RY, Brumfield SK, Bell SD, Young MJ. Functional interplay between a virus and the ESCRT machinery in archaea. *Proc Natl Acad Sci U S A.* 2013; 110:10783–7. [PubMed: 23754419]
32. Frickey T, Lupas AN. Phylogenetic analysis of AAA proteins. *J Struct Biol.* 2004; 146:2–10. [PubMed: 15037233]
33. Iyer LM, Leipe DD, Koonin EV, Aravind L. Evolutionary history and higher order classification of AAA+ ATPases. *J Struct Biol.* 2004; 146:11–31. [PubMed: 15037234]
34. Ogura T, Wilkinson AJ. AAA+ superfamily ATPases: common structure--diverse function. *Genes Cells.* 2001; 6:575–97. [PubMed: 11473577]
35. Kieffer C, Skalicky JJ, Morita E, De Domenico I, Ward DM, Kaplan J, Sundquist WI. Two distinct modes of ESCRT-III recognition are required for VPS4 functions in lysosomal protein targeting and HIV-1 budding. *Dev Cell.* 2008; 15:62–73. [PubMed: 18606141]
36. Stuchell-Brereton MD, Skalicky JJ, Kieffer C, Karren MA, Ghaffarian S, Sundquist WI. ESCRT-III recognition by VPS4 ATPases. *Nature.* 2007; 449:740–4. [PubMed: 17928862]
37. Scott A, Gaspar J, Stuchell-Brereton MD, Alam SL, Skalicky JJ, Sundquist WI. Structure and ESCRT-III protein interactions of the MIT domain of human VPS4A. *Proc Natl Acad Sci U S A.* 2005; 102:13813–8. [PubMed: 16174732]
38. Obita T, Saksena S, Ghazi-Tabatabai S, Gill DJ, Perisic O, Emr SD, Williams RL. Structural basis for selective recognition of ESCRT-III by the AAA ATPase Vps4. *Nature.* 2007; 449:735–9. [PubMed: 17928861]
39. Azmi I, Davies B, Dimaano C, Payne J, Eckert D, Babst M, Katzmann DJ. Recycling of ESCRTs by the AAA-ATPase Vps4 is regulated by a conserved VSL region in Vta1. *J Cell Biol.* 2006; 172:705–17. [PubMed: 16505166]
40. Scott A, Chung HY, Gonciarz-Swiatek M, Hill GC, Whitby FG, Gaspar J, Holton JM, Viswanathan R, Ghaffarian S, Hill CP, Sundquist WI. Structural and mechanistic studies of VPS4 proteins. *EMBO J.* 2005; 24:3658–69. [PubMed: 16193069]
41. Yang D, Hurley JH. Structural role of the Vps4-Vta1 interface in ESCRT-III recycling. *Structure.* 2010; 18:976–84. [PubMed: 20696398]
42. Lottridge JM, Flannery AR, Vincelli JL, Stevens TH. Vta1p and Vps46p regulate the membrane association and ATPase activity of Vps4p at the yeast multivesicular body. *Proc Natl Acad Sci U S A.* 2006; 103:6202–7. [PubMed: 16601096]
43. Xiao J, Xia H, Zhou J, Azmi IF, Davies BA, Katzmann DJ, Xu Z. Structural basis of Vta1 function in the multivesicular body sorting pathway. *Dev Cell.* 2008; 14:37–49. [PubMed: 18194651]
44. Babst M, Wendland B, Estepa EJ, Emr SD. The Vps4p AAA ATPase regulates membrane association of a Vps protein complex required for normal endosome function. *EMBO J.* 1998; 17:2982–93. [PubMed: 9606181]
45. Gonciarz MD, Whitby FG, Eckert DM, Kieffer C, Heroux A, Sundquist WI, Hill CP. Biochemical and structural studies of yeast Vps4 oligomerization. *J Mol Biol.* 2008; 384:878–95. [PubMed: 18929572]
46. Hartmann C, Chami M, Zachariae U, de Groot BL, Engel A, Grutter MG. Vacuolar protein sorting: two different functional states of the AAA-ATPase Vps4p. *J Mol Biol.* 2008; 377:352–63. [PubMed: 18272179]
47. Landsberg MJ, Vajjhala PR, Rothnagel R, Munn AL, Hankamer B. Three-dimensional structure of AAA ATPase Vps4: advancing structural insights into the mechanisms of endosomal sorting and enveloped virus budding. *Structure.* 2009; 17:427–37. [PubMed: 19278657]

48. Xiao J, Xia H, Yoshino-Koh K, Zhou J, Xu Z. Structural characterization of the ATPase reaction cycle of endosomal AAA protein Vps4. *J Mol Biol.* 2007; 374:655–70. [PubMed: 17949747]
49. Inoue M, Kamikubo H, Kataoka M, Kato R, Yoshimori T, Wakatsuki S, Kawasaki M. Nucleotide-dependent conformational changes and assembly of the AAA ATPase SKD1/VPS4B. *Traffic.* 2008; 9:2180–9. [PubMed: 18796009]
50. Roll-Mecak A, Vale RD. Structural basis of microtubule severing by the hereditary spastic paraplegia protein spastin. *Nature.* 2008; 451:363–7. [PubMed: 18202664]
51. Davies JM, Brunger AT, Weis WI. Improved structures of full-length p97, an AAA ATPase: implications for mechanisms of nucleotide-dependent conformational change. *Structure.* 2008; 16:715–26. [PubMed: 18462676]
52. Dreveny I, Kondo H, Uchiyama K, Shaw A, Zhang X, Freemont PS. Structural basis of the interaction between the AAA ATPase p97/VCP and its adaptor protein p47. *EMBO J.* 2004; 23:1030–9. [PubMed: 14988733]
53. Huyton T, Pye VE, Briggs LC, Flynn TC, Beuron F, Kondo H, Ma J, Zhang X, Freemont PS. The crystal structure of murine p97/VCP at 3.6Å. *J Struct Biol.* 2003; 144:337–48. [PubMed: 14643202]
54. Zhang X, Shaw A, Bates PA, Newman RH, Gowen B, Orlova E, Gorman MA, Kondo H, Dokurno P, Lally J, Leonard G, Meyer H, van Heel M, Freemont PS. Structure of the AAA ATPase p97. *Mol Cell.* 2000; 6:1473–84. [PubMed: 11163219]
55. Yu Z, Gonciarz MD, Sundquist WI, Hill CP, Jensen GJ. Cryo-EM structure of dodecameric Vps4p and its 2:1 complex with Vta1p. *J Mol Biol.* 2008; 377:364–77. [PubMed: 18280501]
56. Story RM, Steitz TA. Structure of the recA protein-ADP complex. *Nature.* 1992; 355:374–6. [PubMed: 1731253]
57. Wendler P, Ciniawsky S, Kock M, Kube S. Structure and function of the AAA+ nucleotide binding pocket. *Biochim Biophys Acta.* 2012; 1823:2–14. [PubMed: 21839118]
58. Moriscot C, Gribaldo S, Jault JM, Krupovic M, Arnaud J, Jamin M, Schoehn G, Forterre P, Weissenhorn W, Renesto P. Crenarchaeal CdvA Forms Double-Helical Filaments Containing DNA and Interacts with ESCRT-III-Like CdvB. *PLoS One.* 2011; 6:e21921. [PubMed: 21760923]
59. Brock TD, Brock KM, Belly RT, Weiss RL. *Sulfolobus*: a new genus of sulfur-oxidizing bacteria living at low pH and high temperature. *Archiv fur Mikrobiologie.* 1972; 84:54–68. [PubMed: 4559703]
60. Janin J, Bahadur RP, Chakrabarti P. Protein-protein interaction and quaternary structure. *Quarterly reviews of biophysics.* 2008; 41:133–80. [PubMed: 18812015]
61. Wang Q, Song C, Irizarry L, Dai R, Zhang X, Li CC. Multifunctional roles of the conserved Arg residues in the second region of homology of p97/valosin-containing protein. *J Biol Chem.* 2005; 280:40515–23. [PubMed: 16216872]
62. Davies BA, Azmi IF, Payne J, Shestakova A, Horazdovsky BF, Babst M, Katzmann DJ. Coordination of substrate binding and ATP hydrolysis in Vps4-mediated ESCRT-III disassembly. *Mol Biol Cell.* 2010; 21:3396–408. [PubMed: 20702581]
63. Azmi IF, Davies BA, Xiao J, Babst M, Xu Z, Katzmann DJ. ESCRT-III family members stimulate Vps4 ATPase activity directly or via Vta1. *Dev Cell.* 2008; 14:50–61. [PubMed: 18194652]
64. Merrill SA, Hanson PI. Activation of human VPS4A by ESCRT-III proteins reveals ability of substrates to relieve enzyme autoinhibition. *J Biol Chem.* 2010; 285:35428–38. [PubMed: 20805225]
65. Erzberger JP, Berger JM. Evolutionary relationships and structural mechanisms of AAA+ proteins. *Annu Rev Biophys Biomol Struct.* 2006; 35:93–114. [PubMed: 16689629]
66. Hanson PI, Whiteheart SW. AAA+ proteins: have engine, will work. *Nat Rev Mol Cell Biol.* 2005; 6:519–29. [PubMed: 16072036]
67. Lupas AN, Martin J. AAA proteins. *Curr Opin Struct Biol.* 2002; 12:746–53. [PubMed: 12504679]
68. Akoev V, Gogol EP, Barnett ME, Zolkiewski M. Nucleotide-induced switch in oligomerization of the AAA+ ATPase ClpB. *Protein Sci.* 2004; 13:567–74. [PubMed: 14978298]
69. Zhang F, Hu M, Tian G, Zhang P, Finley D, Jeffrey PD, Shi Y. Structural insights into the regulatory particle of the proteasome from *Methanocaldococcus jannaschii*. *Mol Cell.* 2009; 34:473–84. [PubMed: 19481527]

70. Smith DM, Kafri G, Cheng Y, Ng D, Walz T, Goldberg AL. ATP binding to PAN or the 26S ATPases causes association with the 20S proteasome, gate opening, and translocation of unfolded proteins. *Mol Cell*. 2005; 20:687–98. [PubMed: 16337593]
71. Henderson JN, Hazra S, Dunkle AM, Salvucci ME, Wachter RM. Biophysical characterization of higher plant Rubisco activase. *Biochim Biophys Acta*. 2013; 1834:87–97. [PubMed: 22985719]
72. Stotz M, Mueller-Cajar O, Ciniawsky S, Wendler P, Hartl FU, Bracher A, Hayer-Hartl M. Structure of green-type Rubisco activase from tobacco. *Nat Struct Mol Biol*. 2011; 18:1366–70. [PubMed: 22056769]
73. Enemark EJ, Joshua-Tor L. Mechanism of DNA translocation in a replicative hexameric helicase. *Nature*. 2006; 442:270–5. [PubMed: 16855583]
74. Thomsen ND, Berger JM. Running in reverse: the structural basis for translocation polarity in hexameric helicases. *Cell*. 2009; 139:523–34. [PubMed: 19879839]
75. Diemand AV, Lupas AN. Modeling AAA+ ring complexes from monomeric structures. *J Struct Biol*. 2006; 156:230–43. [PubMed: 16765605]
76. Cormier CY, Park JG, Fiocco M, Steel J, Hunter P, Kramer J, Singla R, LaBaer J. PSI:Biologymaterials repository: a biologist's resource for protein expression plasmids. *Journal of structural and functional genomics*. 2011; 12:55–62. [PubMed: 21360289]
77. Otwinowski, Z.; Minor, W. Processing of X-ray diffraction data collected in oscillation mode. In: Carter, J.; CW; Sweet, RM., editors. *Methods Enzymol*. Vol. 276. Academic Press; New York: 1997. p. 307-326.
78. Terwilliger TC, Berendzen J. Automated MAD and MIR structure solution. *Acta Crystallogr D Biol Crystallogr*. 1999; 55:849–61. [PubMed: 10089316]
79. McCoy AJ, Grosse-Kunstleve RW, Storoni LC, Read RJ. Likelihood-enhanced fast translation functions. *Acta Crystallogr D Biol Crystallogr*. 2005; 61:458–64. [PubMed: 15805601]
80. Murshudov GN, Vagin AA, Dodson EJ. Refinement of macromolecular structures by the maximum-likelihood method. *Acta Crystallogr D Biol Crystallogr*. 1997; 53:240–55. [PubMed: 15299926]
81. Emsley P, Cowtan K. Coot: model-building tools for molecular graphics. *Acta Crystallogr D Biol Crystallogr*. 2004; 60:2126–32. [PubMed: 15572765]
82. Krissinel E, Henrick K. Inference of macromolecular assemblies from crystalline state. *J Mol Biol*. 2007; 372:774–97. [PubMed: 17681537]
83. Krissinel E, Henrick K. Secondary-structure matching (SSM), a new tool for fast protein structure alignment in three dimensions. *Acta Crystallogr D Biol Crystallogr*. 2004; 60:2256–68. [PubMed: 15572779]
84. Winn MD, Ballard CC, Cowtan KD, Dodson EJ, Emsley P, Evans PR, Keegan RM, Krissinel EB, Leslie AG, McCoy A, McNicholas SJ, Murshudov GN, Pannu NS, Potterton EA, Powell HR, Read RJ, Vagin A, Wilson KS. Overview of the CCP4 suite and current developments. *Acta Crystallogr D Biol Crystallogr*. 2011; 67:235–42. [PubMed: 21460441]
85. DeLano, WL. The PyMOL Molecular Graphics System. DeLano Scientific; San Carlos, CA, USA: 2002.
86. Cole JL, Lary JW, TPM, Laue TM. Analytical ultracentrifugation: sedimentation velocity and sedimentation equilibrium. *Methods Cell Biol*. 2008; 84:143–79. [PubMed: 17964931]
87. Cole JL. Analysis of heterogeneous interactions. *Methods Enzymol*. 2004; 384:212–32. [PubMed: 15081689]
88. Laue, TM.; Shah, BD.; Ridgeway, TM.; Pelletier, SL. Analytical Ultracentrifugation in Biochemistry and Polymer Science. Harding, S.; Rowe, A.; Horton, J., editors. Royal Society of Chemistry; Cambridge: 1992. p. 90-125.

Highlights

- The Vps4 AAA ATPase is required for ESCRT-mediated membrane fission.
- Wild-type Vps4 proteins across species are hexamers in the presence of nucleotides.
- Hexamer interfaces are conserved between eukaryotic and archaeal Vps4 proteins.
- A commonly used hydrolysis mutant assembles into non-native complexes.
- In contrast to previous double-ring models, active Vps4 is a single-ring hexamer.

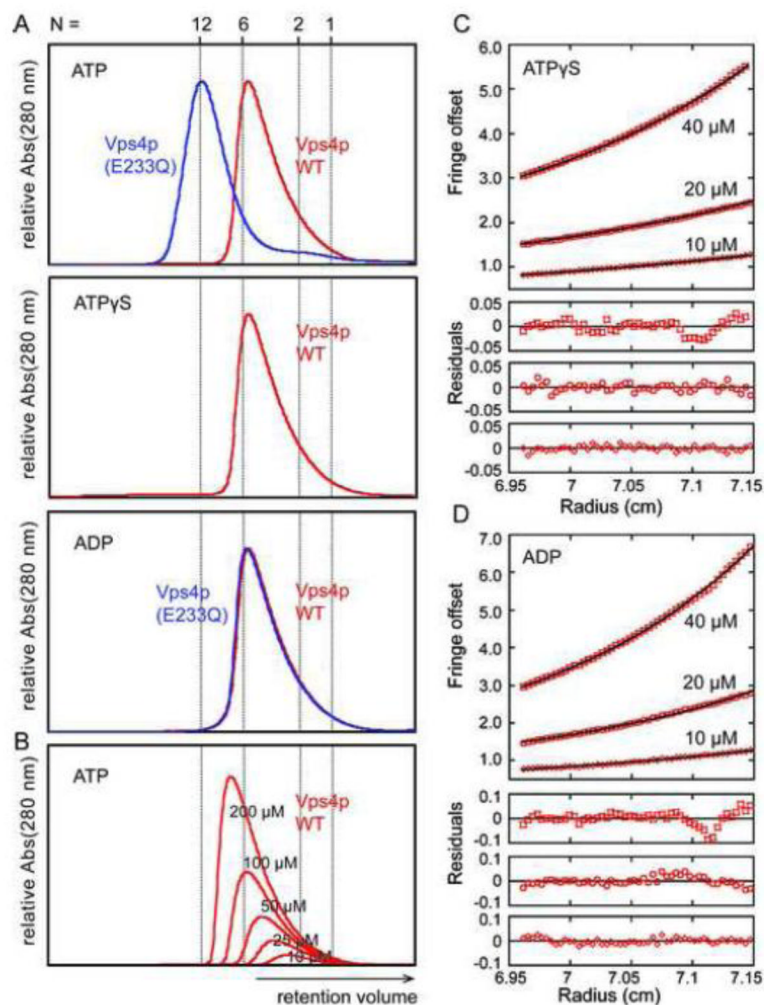


Figure 1. Oligomerization of *S. cerevisiae* Vps4p proteins. (A) Size exclusion chromatograms of wild-type Vps4p (red) and Vps4p(E233Q) (blue), injected at a concentration of 100 μ M, in the presence of 2 mM magnesium chloride and 1 mM ATP, 0.2 mM ATP γ S, or 1 mM ADP. Expected retention volumes for different oligomeric states of Vps4p based on molecular weight standards are indicated with dotted lines. Note that Vps4p(E233Q) elutes as a dodecamer in the presence of ATP, but as a hexamer in the presence of ADP, whereas wild-type Vps4p elutes as a hexamer in the presence of ATP, ATP γ S or ADP. (B) Size exclusion chromatograms of wild-type Vps4p at concentrations ranging from 10 μ M to 200 μ M in the presence of 1 mM ATP. Note that the complex migrates more slowly at lower concentrations, indicating that Vps4p is in a rapid equilibrium between different oligomeric states. (C, D) Equilibrium analytical ultracentrifugation at 4 $^{\circ}$ C indicates that wild-type Vps4p is in a dimer-hexamer equilibrium in the presence of (C) 1 mM ATP γ S or (D) 1 mM ADP. The interference signal from sedimentation data at 5000 rpm is plotted versus the distance from the axis of rotation (radius) as red symbols. Three different protein concentrations are displayed: 40 μ M (upper), 20 μ M (middle) and 10 μ M (lower). The global fit to data obtained for three concentrations at rotor speeds of 3000 rpm (not shown) and 5000 rpm using a dimer-hexamer model is shown in black with residuals for all three concentrations displayed below.

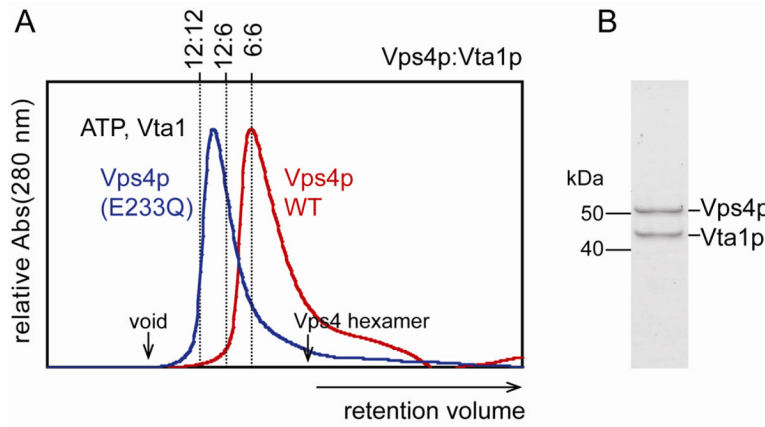


Figure 2.

Wild type Vps4p remains hexameric and Vps4p(E233Q) remains dodecameric in the presence of Vta1p. (A) ATP-bound wild-type and E233Q Vps4p size exclusion chromatograms. Calculated retention volumes for 6:6, 6:12, and 12:12 Vps4p:Vta1p complexes are indicated. The void volume and the expected elution volume for the Vps4p hexamer are indicated by arrows. (B) SDS PAGE analysis of the peak fraction of wild-type Vps4p (48 kDa) in the presence of Vta1p (37 kDa) confirms that the peak represents a complex of both proteins.

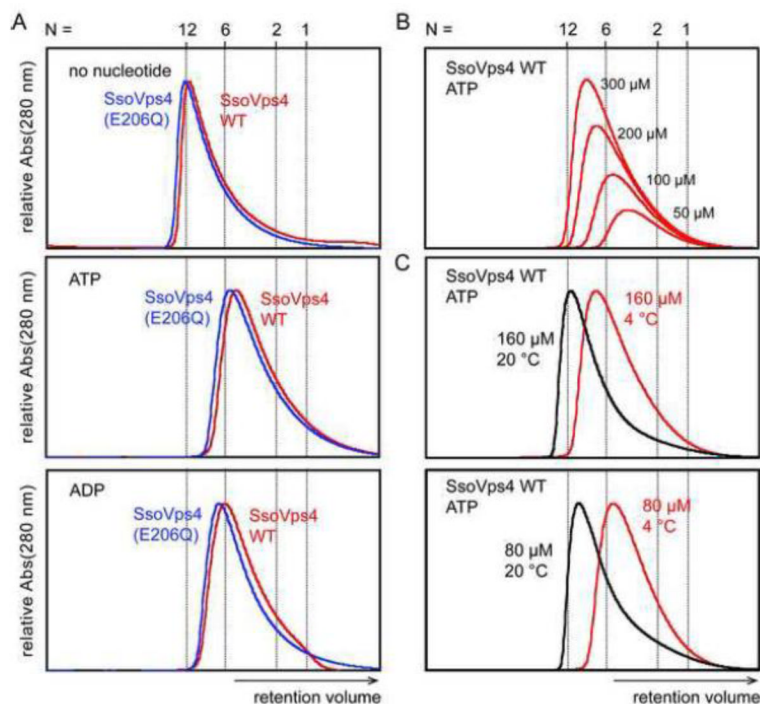


Figure 3. Characterization of SsoVps4 oligomerization by size exclusion chromatography. (A) Chromatograms of SsoVps4 (red) and SsoVps4(E206Q) (blue) injected at concentrations of 100 μ M. Both proteins eluted as dodecamers in the absence of nucleotide but eluted as hexamers when the buffer was supplemented with 2 mM magnesium chloride and 1 mM ATP or ADP. (B) Chromatograms of different concentrations of SsoVps4. The shift in retention volume following injection at different protein concentrations indicates that SsoVps4 rapidly interconverts between multiple oligomeric states. (C) A shift of temperature from 4 $^{\circ}$ C (red) to 20 $^{\circ}$ C (black) reduces the elution volume: 160 μ M (upper) and 80 μ M (lower). Standard molecular weight markers displayed very similar retention volumes at the two temperatures.

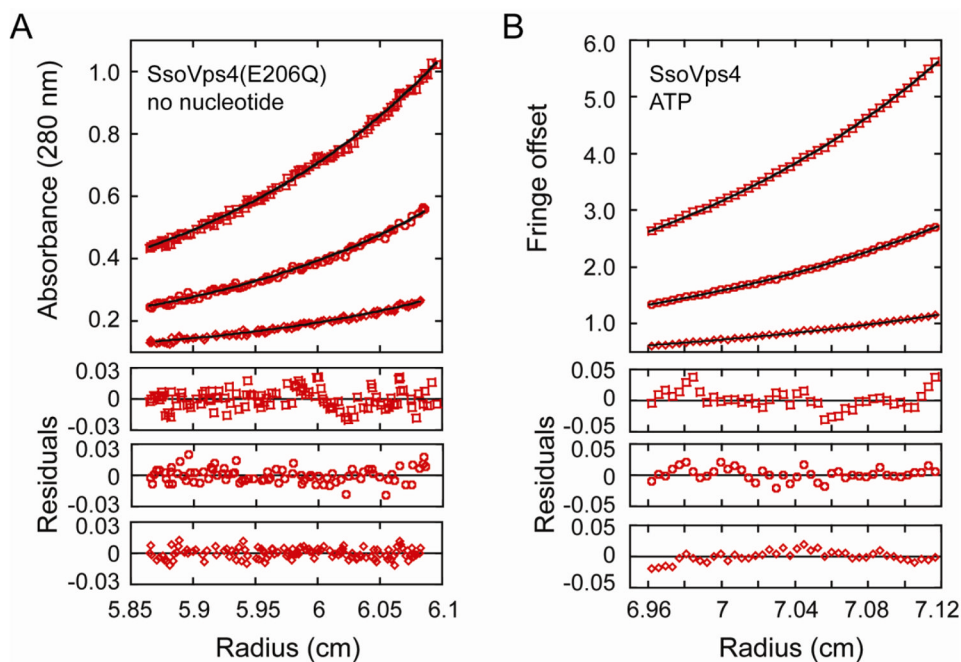


Figure 4. Characterization of SsoVps4 oligomerization by equilibrium analytical ultracentrifugation. (A) SsoVps4(E206Q) in the absence of nucleotide. Data are shown from a 3500 rpm spin at three protein concentrations: 10 μ M (upper), 5 μ M (middle) and 2.5 μ M (lower). The black line corresponds to an ideal species fit for dodecameric SsoVps4. Residuals are displayed below. (B) Wild-type SsoVps4 in the presence of 1 mM ATP at 5000 rpm. Three different protein concentrations are displayed: 47 μ M (upper), 24 μ M (middle) and 12 μ M (lower). Interference scans at 3000 rpm for all concentrations were also included in the fit, but are not shown here. The fit obtained using a dimer-hexamer model is shown in black.

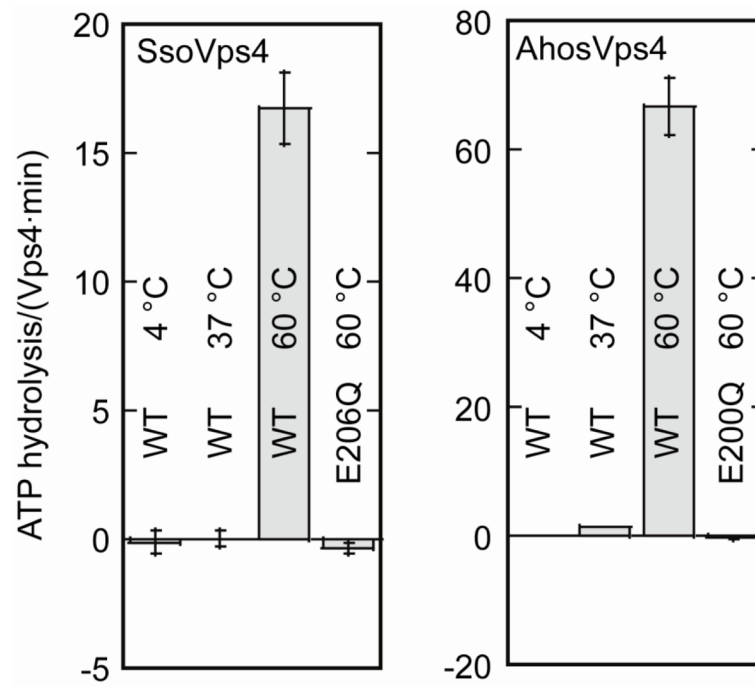


Figure 5. ATPase activity of SsoVps4 and AhosVps4 at 4 °C, 37 °C and 60 °C. Both proteins are active at 60 °C. Mutation of the Walker B glutamate in SsoVps4(E206Q) or AhosVps4(E200Q) abolishes ATPase activity.

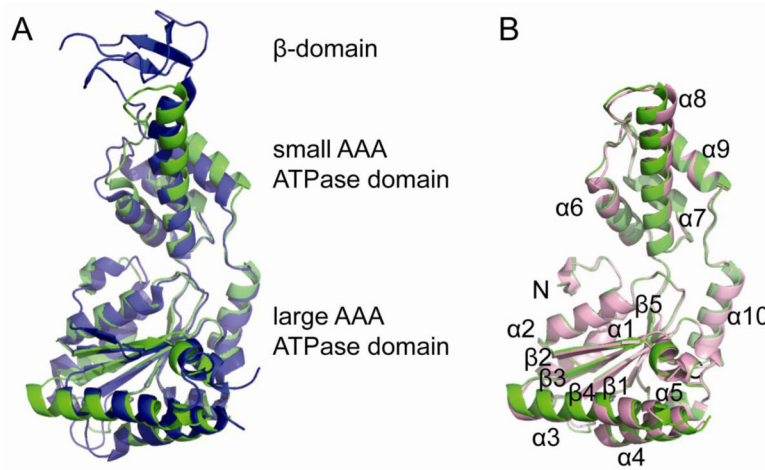


Figure 6.

Crystal structures of the ATPase cassettes of SsoVps4 and AhoVps4. (A) Superposition of SsoVps4 (green) and Vps4p (PDB ID: 3EIE⁴⁵, blue) yields an RMSD of 1.622 Å over 237 pairs of Ca atoms. (B) The structures of SsoVps4 (green) and AhoVps4 (pink) overlay with an RMSD of 0.492 Å on 206 pairs of Ca atoms.

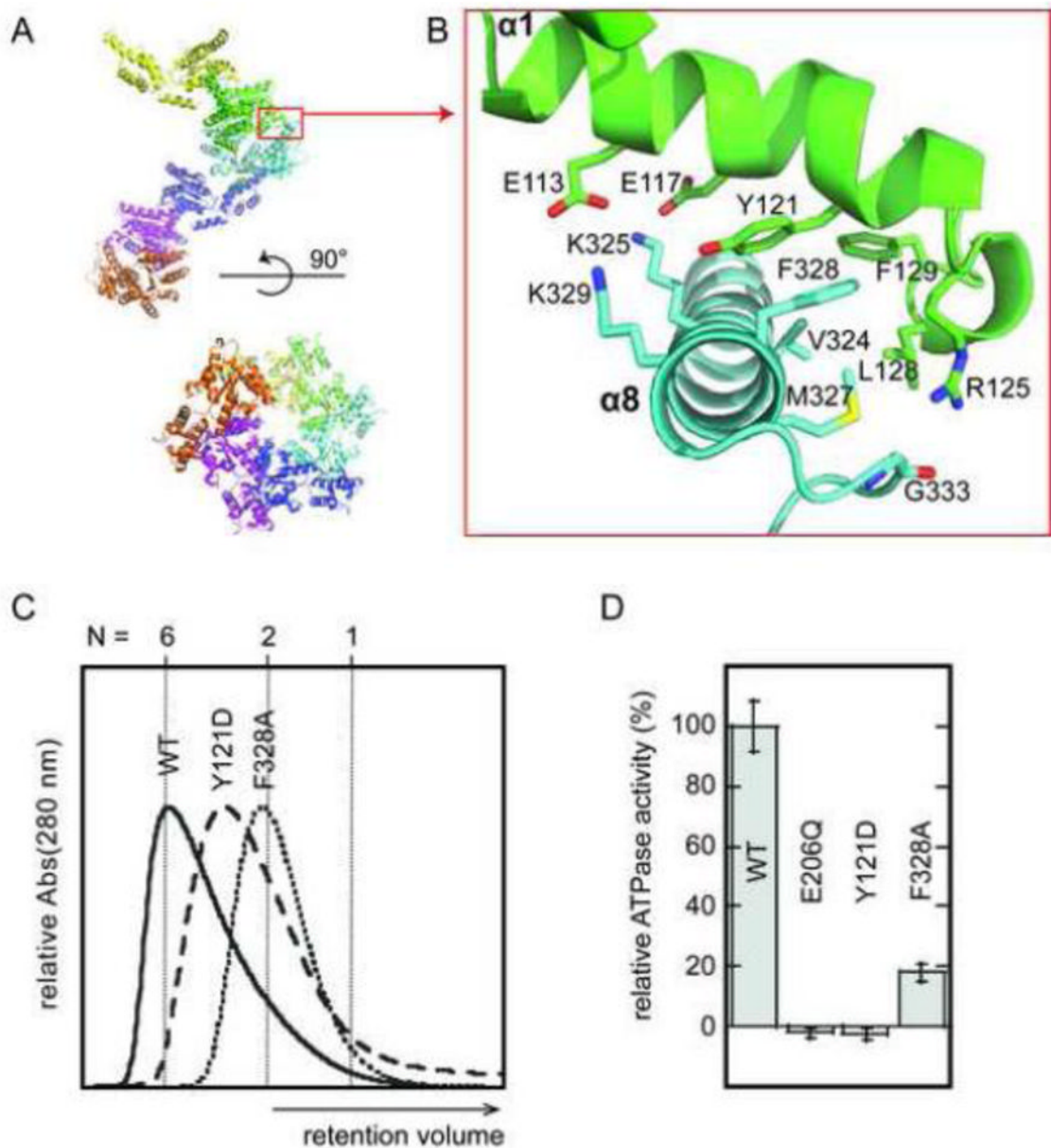


Figure 7. The crystallographic interface between SsoVps4 molecules related by a 6_4 screw axis provides a model for the hexamer interface in solution. (A) Six symmetry-related molecules shown in separate colors viewed along (lower) and perpendicular to (upper) the 6_4 screw axis. (B) Detailed view of the contact boxed in panel A. Contacting residues are labeled and shown as sticks. Y121 and F328 form a π -stacking interaction at the center of the interface. (C) Size exclusion chromatograms of wild-type SsoVps4, SsoVps4(Y121D) and SsoVps4(F328A) in the presence of 1 mM ATP. (D) SsoVps4 ATPase activity assays performed at 60°C.

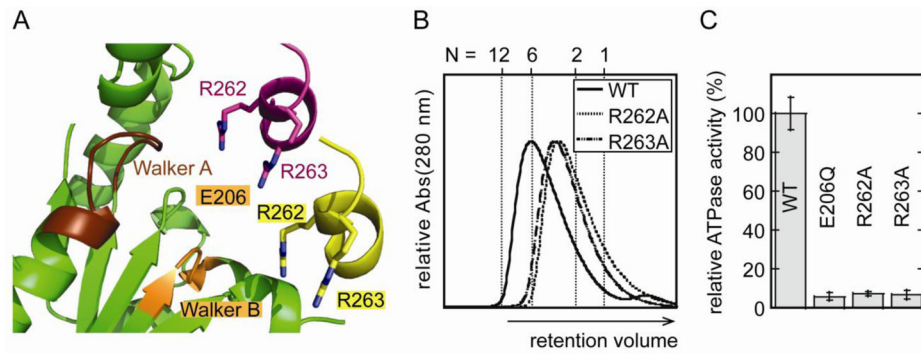


Figure 8. Arginine finger residues contribute to Vps4 oligomerization and are important for ATPase activity. (A) The nucleotide binding site of SsoVps4 (green) contains the conserved Walker A (brown), Walker B (orange) motifs. The neighboring subunit in the crystal is shown in yellow, and its position in the p97-like hexamer model is shown in magenta. Glutamate 206 and the potential arginine finger residues 262 and 263 are shown in stick representation. (B) Point mutations R262A and R263A destabilize the oligomer and (C) abolish ATPase activity.

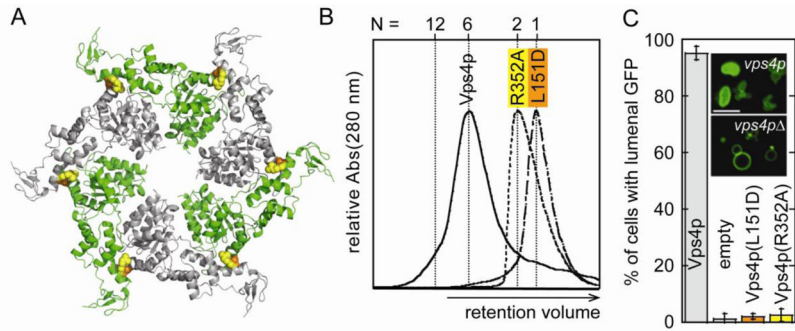


Figure 9. Mutational analysis of the hexamer interface in yeast Vps4p. (A) L151 (orange spheres) and R352 (yellow spheres) map to the hexamer interface in the p97-like ring. (B) Vps4p(R352A) and Vps4p(L151D) do not form higher-order oligomers as shown by size exclusion chromatography in the presence of 1 mM ATP. (C) Vacuolar protein sorting of the model cargo CPS-GFP into the vacuole lumen is severely impaired in yeast cells expressing interface mutants Vps4p(L151D) or Vps4p(R352A) as compared to cells containing wild-type Vps4p. Insets show control examples of successful (upper) and unsuccessful (lower) CPS-GFP sorting.

Table 1

X-ray data collection and refinement statistics

	SsoVps4(E206Q, 85-372)	AhosVps4
<i>Data Collection</i>		
Beamline	SSRL 7-1	SSRL 11-1
Wavelength (Å)	0.97945	0.9795
Resolution range (Å)	30 - 2.73 (2.83 - 2.73)	30 - 2.1 (2.18 - 2.1)
Space group	P6 ₄	P6 ₅
Cell parameters (Å)	a=101.3 c=64.7	a=96.0 c=79.5
Total observations	113,696	229,024
Unique observations	9,896	24,620
Completeness (%)	98.6 (92.0)	98.9 (98.4)
$\langle I \rangle / \sigma(I)$	25.2 (7.8)	13.5 (4.5)
R _{sym}	0.073 (0.657)	0.083 (0.673)
<i>Refinement</i>		
R _{work} /R _{free} (%)	22.9/26.8	21.4/25.6
RMSD from ideal geometry		
- Bond lengths (Å)	0.006	0.017
- Bond angles (°)	1.4	1.4
Average B-factor (Å ²)	98.0	46.7
Ramachandran favored (%)	98.7	99.6
Ramachandran outliers (%)	0	0

Values in parentheses refer to the high resolution shell.